Supporting information

Rational Screening of Milling Parameters for Ru-Na/Al_2O_3 Dual-Function Materials for the Integrated CO_2 Capture and Methanation

Andrea Braga, Maila Danielis*, Sara Colussi, Alessandro Trovarelli

Dipartimento Politecnico e INSTM, Università degli Studi di Udine, 33100 Udine, Italy

*maila.danielis@uniud.it

CO_2 capture estimation

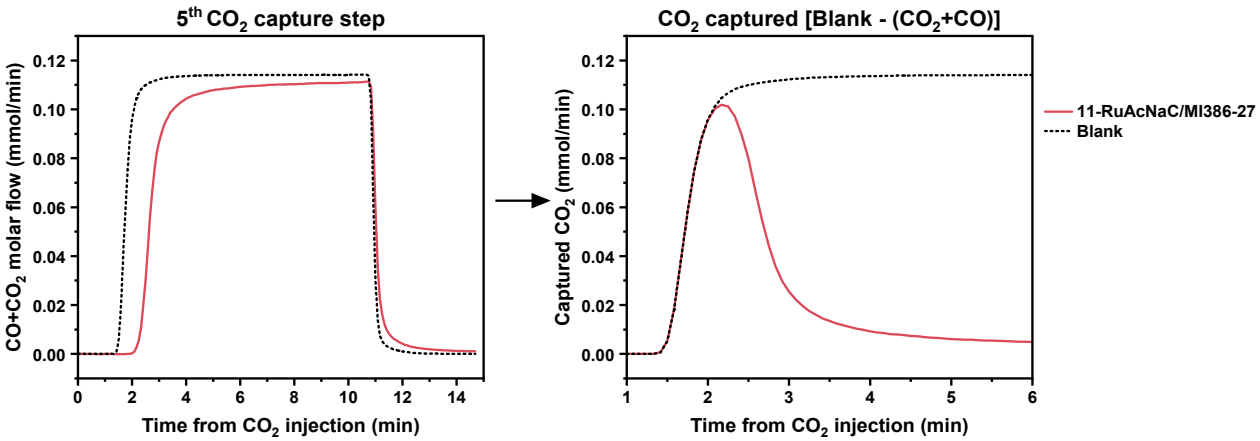

Figure S1. Graphical representation of the CO_2 capture capacity estimation as the difference between the blank 5% CO_2 signal and the CO_2 measured from the sample.

Preliminary evaluation of alkali-support oxide binary systems

A series of Na_2O/Al_2O_3 samples were initially prepared by milling Na_2CO_3 or $NaNO_3$ with MI386 at different loadings and milling intensities. These samples were characterised by XRD, porosimetry and TGA decomposition in air to assess the morphology and the modifications induced by the different milling regimes on the Na species.

Different milling regimes and Na_2O equivalent loading were tested. The optimal Na_2O equivalent loading was 10%, while the maximum milling frequency was set at 35 Hz, as higher Na loadings and milling frequencies resulted in materials with unsatisfactory morphological properties. In the ranges from 15 to 35 Hz, and from 15 to 35 min, the properties of 10%Na_2O/MI386 materials showed a good variability; milling frequencies higher than 35 Hz and longer milling times resulted in materials with unsatisfactory morphological properties. Also, Na_2O loadings higher than 10% were attempted to try and increase the capture capacity of the DFMs. However, these samples resulted in materials with too low surface area and no pore structure. For these reasons, a series of 10%Na_2O/Al_2O_3 was prepared by milling 16 wt% of Na_2CO_3 and 23 wt% of $NaNO_3$ with MI386 (NaC/MI386 and NaN/MI386) at various milling times and frequencies in the range of 15 to 35 Hz for 15 to 35 min.

Table S1. BET surface area and BJH pore size and volume of the Na/MI386 samples milled at different intensities. The equivalent Na_2O loading is 10 wt%. achieved by milling 16 wt% of Na_2CO_3 or 23 wt% of $NaNO_3$.

Sample	BET Surface area (m^2/g)	BJH Pore diameter (nm)	BJH Pore volume (cm^3/g)
MI386	173	9	0.77
16%NaC/MI386-15	138	9	0.59
30%NaC/MI386-15	113	9	0.50
16%NaC/MI386-27	120	6	0.35
23%NaC/MI386-27	77	5	0.23
30%NaC/MI386-27	51	6	0.15
16%NaC/MI386-35	73	6	0.17
30%NaC/MI386-50	11	4	0.04
23%NaN/MI386-15	120	9	0.46
23%NaN/MI386-27	77	5	0.23
23%NaN/MI386-35	34	4	0.10

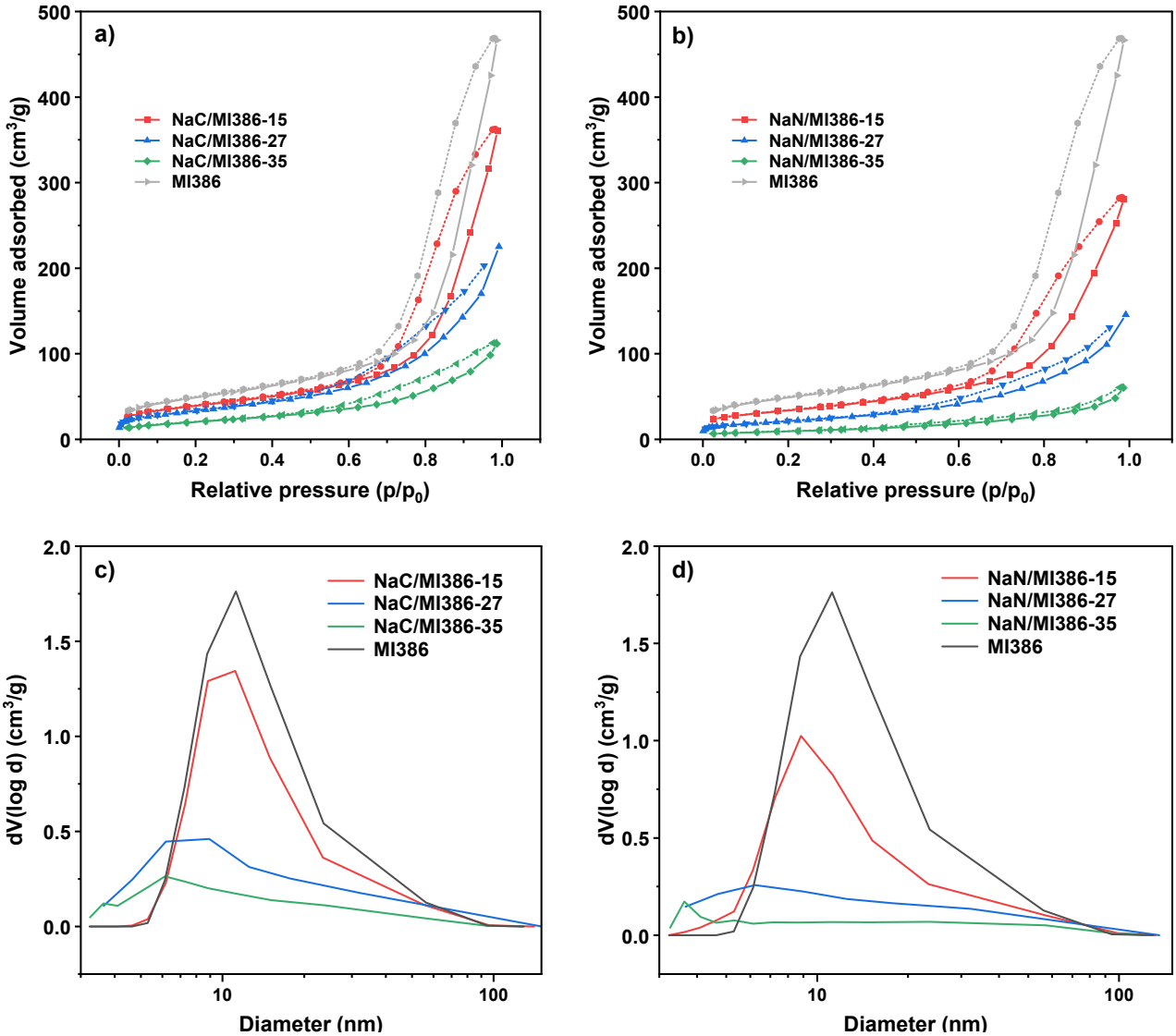

Figure S2. N_2 adsorption (solid lines)/desorption (dotted lines) isotherms of **a)** NaC/MI386 and **b)** NaN/MI386 milled at different milling intensities. Pore size distribution of **c)** NaC/MI386 and **d)** NaN/MI386 milled at different milling intensities.

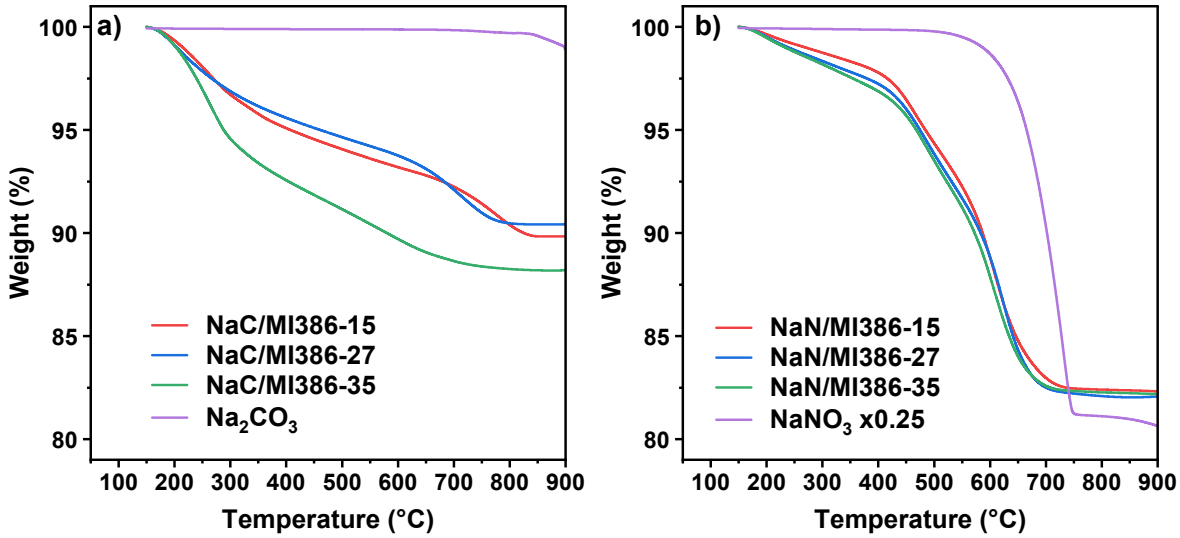

Figure S3. TGA weight profiles in air of the **a)** NaC/MI386 and **b)** NaN/MI386 samples milled at different intensities. The decomposition of pure Na_2CO_3 and $NaNO_3$ are reported for comparison.

At low milling intensity, the Na_2CO_3 decomposition was characterised by two main events centred around 260 and 780 °C, with a shoulder at 350 °C (see also Fig. 1c in the main text). The low-temperature peaks could be associated with Na_2CO_3 in close contact with Al_2O_3, which is reported to favour the decomposition of the carbonate,[1,2] while the high-temperature peak corresponds to the decomposition of bulkier Na_2CO_3 species. For NaC/MI386-27 milled at intermediate milling intensity, the weight loss profile was similar to the NaC/MI386-15 sample, with a shift towards lower temperatures of the low-temperature weight loss (centred around 190 °C) and of the high-temperature peak, shifted from 780 to 700 °C, indicating easier Na_2CO_3 decomposition. The sample NaC/MI386-35 showed a different weight loss profile characterised by a significant loss at 265 °C with a shoulder at 190 °C, and a broad loss event at 625 °C. The total weight loss was comparable for the two samples milled at low and medium regimes, while it was higher for the sample milled at the highest milling intensity. On the latter, the measured weight loss was also higher than the expected loss caused by the sole Na_2CO_3 decomposition to Na_2O, probably due to contributions from Al_2O_3 and gas species adsorbed from the atmosphere. This, in addition to low temperature decomposition behaviour, suggests that at the highest milling intensity most of the Na_2CO_3 is able to form a chemical interaction with Al_2O_3,[1,2] likely promoted by the strong impacts achieved by mechanical forces.

Regarding NaN/MI386 samples, the decomposition pattern was similar among the three samples. Milling NaN with Al_2O_3 changed the decomposition of the nitrates in a two-step process, with a first weight loss at 470 °C and a second more intense loss at 610 °C. However, all samples display the same $NaNO_3$ decomposition behaviour, both in terms of characteristic reduction temperature and final weight loss, regardless of the milling intensity.

RuNa/MI386 DFMs characterisation

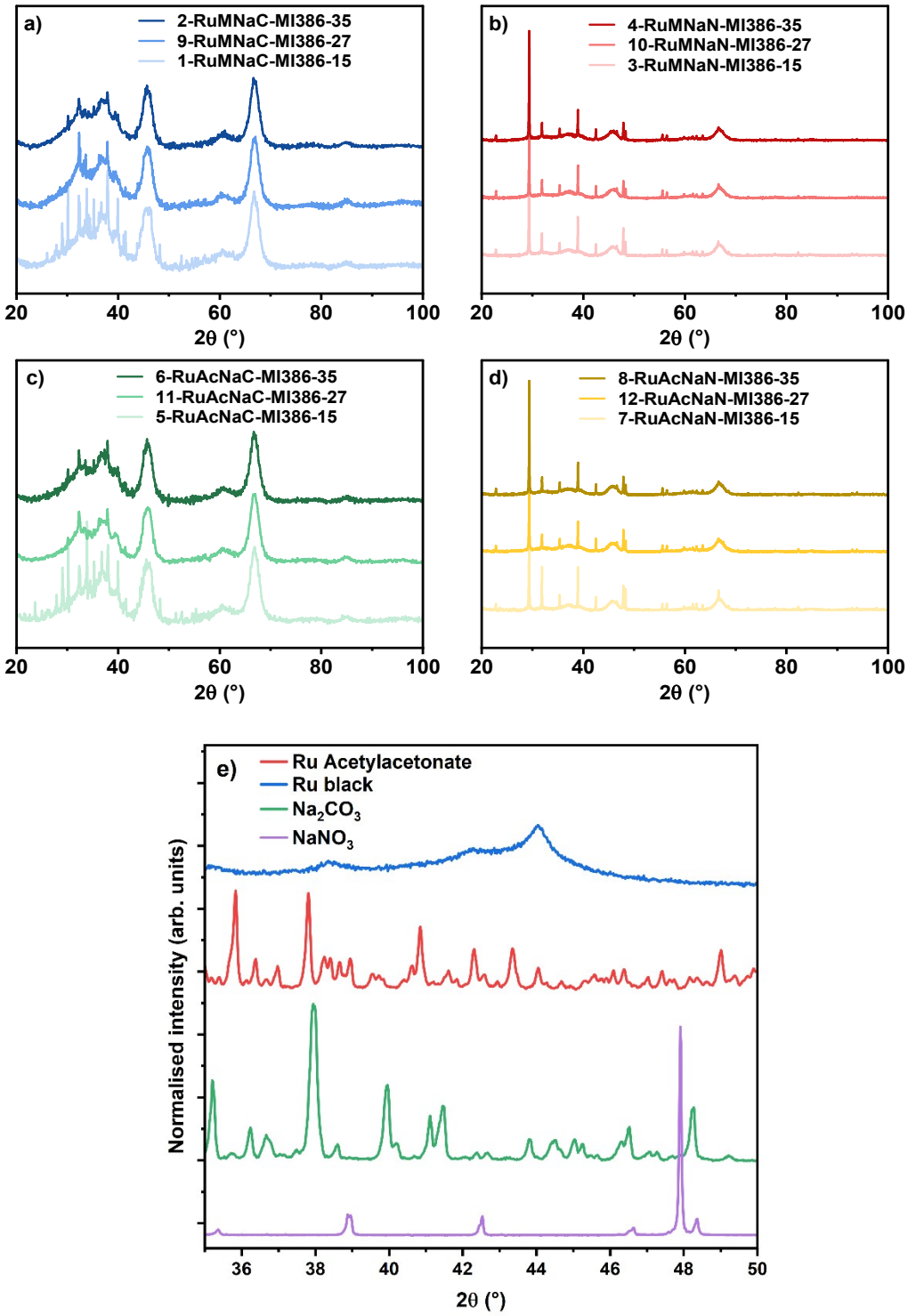

Figure S4. XRD patterns of as-prepared DFMs based on **a)** RuM+Na_2CO_3, **b)** RuM+$NaNO_3$, **c)** RuAc+Na_2CO_3 and **d)** RuAc+$NaNO_3$. In **e)** details of the reference patterns of the different precursors are reported.

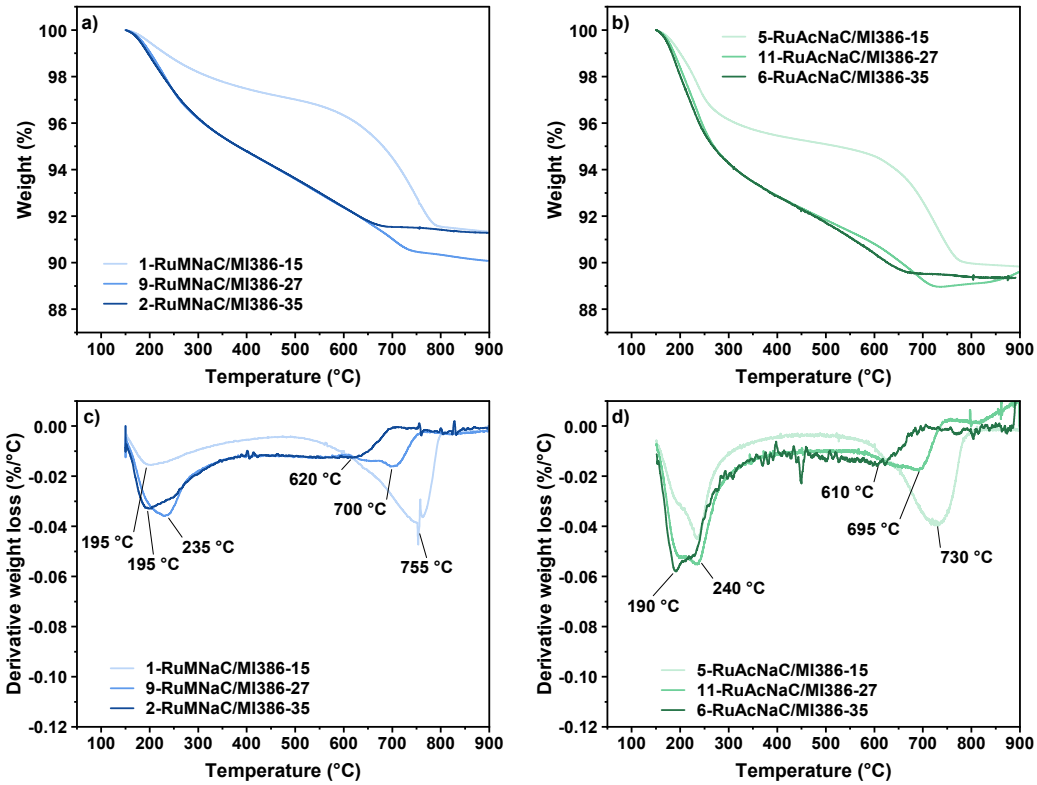

Figure S5. TGA decomposition signals in air of the of Na_2CO_3 of **a)** RuM-DFMs and **b)** the RuAc-DFMs; **c-d)** derivative weight loss signals.

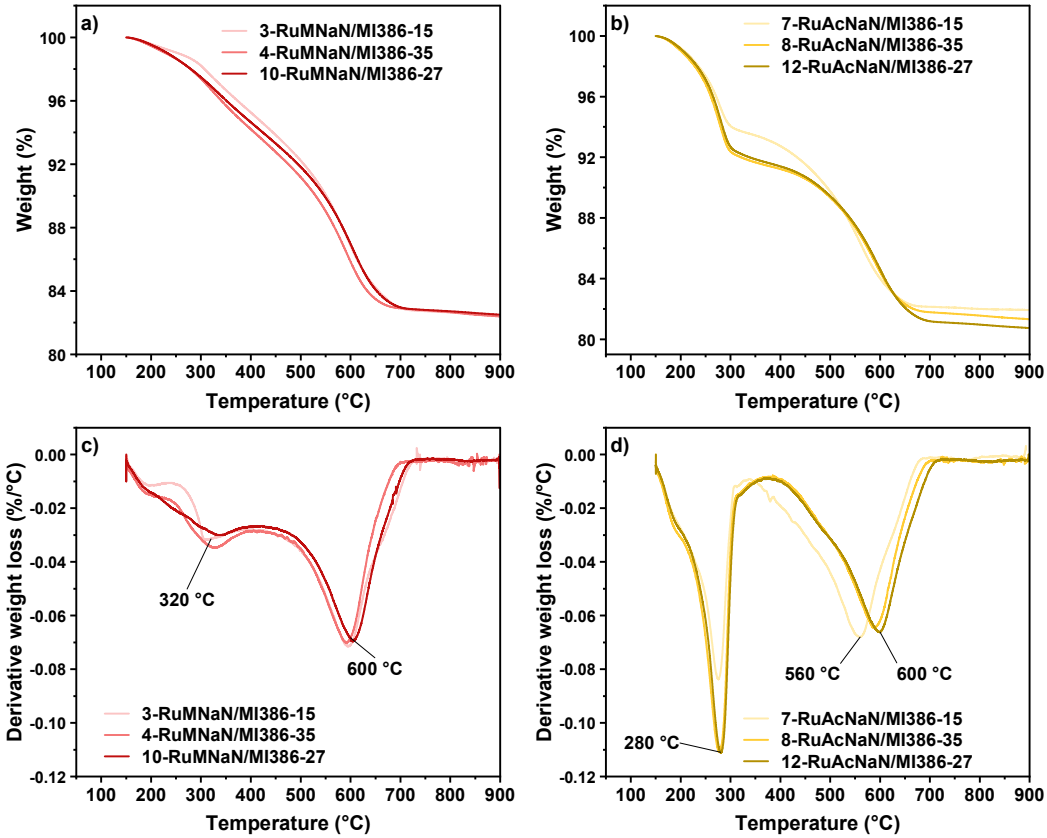

Figure S6. TGA signals of the decomposition in air of $NaNO_3$ on **a)** the DFMs based on Ru metal and **b)** the DFMs based on RuAc; **c-d)** derivative weight loss signals.

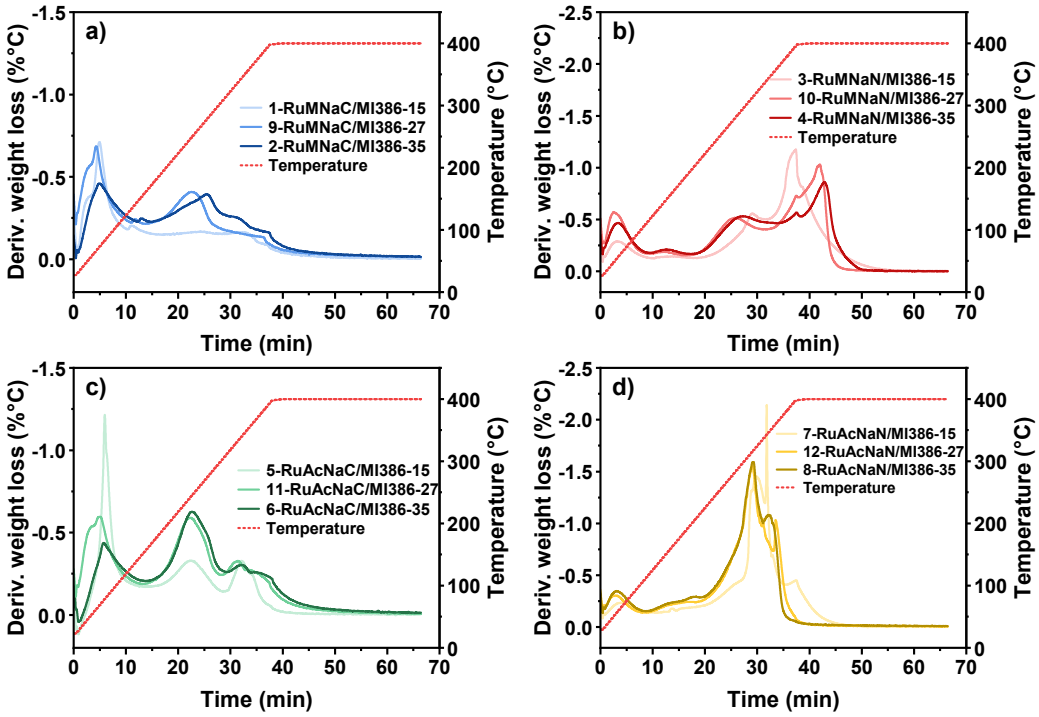

Figure S7. Derivative of the TGA weight loss profile reported in Figure 3 representing the DFMs activation in 5%H_2/N_2. DFMs based on **a)** RuM+Na_2CO_3, **b)** RuM+$NaNO_3$, **c)** RuAc+Na_2CO_3 and **d)** RuAc+$NaNO_3$.

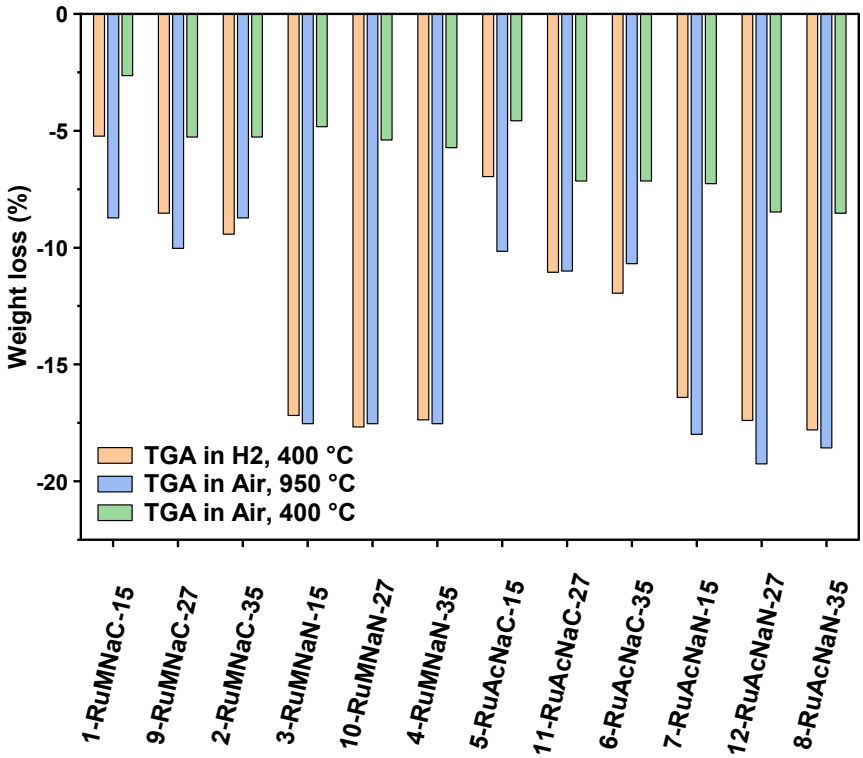

Figure S8. Weight losses at different temperatures and atmospheres as measured by TGA analysis.

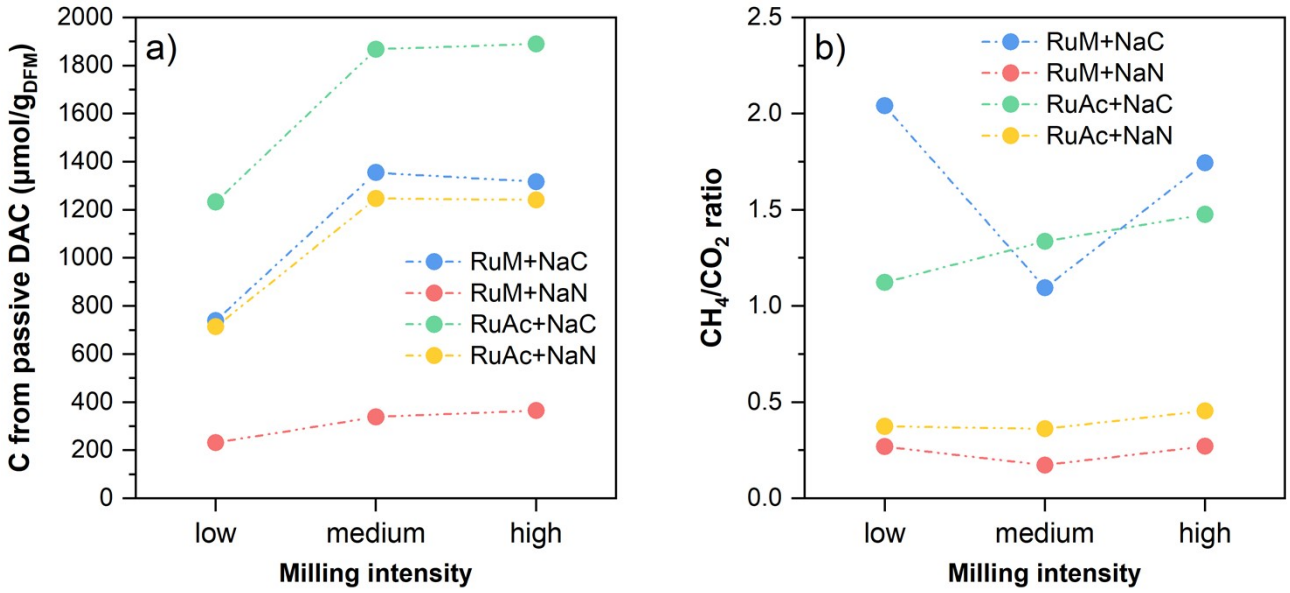

Figure S9. a) Amount of C species from passive DAC reported in Table 2 and **b)** overall CH_4 to CO_2 ratio measured during H_2 activation treatment for all DFMs (10 °C/min to 400 °C, iso 1 h, 10% H_2/N_2, 50 mL/min, 250 mg).

ICCU-MET testing results and analysis

Table S2. Results of the integrated carbon capture and methanation tests as the average of the five cycles at 350 °C. CO_2 capture step: 50 mL/min, 5% CO_2, 10 min; methanation step: 50 mL/min, 10% H_2, 10 min; 250 mg of DFM.

#	Sample	CO_2 capture capacity[a]	Total CH_4 production	CO_2/m^2	CH_4/m^2	CO_2 conversion[b]	CH_4 release rate	CH_4 selectivity[d]	CO produced during capture	CO_2 released during methanation	CO_2 lost during methanation
		µmol/g_{DFM}	µmol/g_{DFM}	µmol/m^2	µmol/m^2	%	µmol/g_{DFM}/min	%	µmol/g_{DFM}	µmol/g_{DFM}	%
1	RuMNaC/MI386-15	233.0	186.9	n.a.	n.a.	85.6	14.5	91.2	45.1	11.6	5.0%
9	RuMNaC/MI386-27	270.2	112.8	n.a.	n.a.	51.9	7.0	66.8	51.5	27.0	10.0%
2	RuMNaC/MI386-35	418.5	240.2	n.a.	n.a.	62.5	11.0	89.3	53.2	18.0	4.3%
3	RuMNaN/MI386-15	258.5	194.5	n.a.	n.a.	80.5	10.7	89.5	45.3	16.2	6.2%
10	RuMNaN/MI386-27	257.8	136.7	n.a.	n.a.	59.3	7.8	84.2	49.2	12.4	4.8%
4	RuMNaN/MI386-35	259.9	139.9	n.a.	n.a.	61.2	7.9	84.0	29.2	14.4	5.6%
5	RuAcNaC/MI386-15	154.4	170.8	1.1	1.2	115.7	85.3	97.2	29.4	4.6	3.0%
11	RuAcNaC/MI386-27	420.6	321.8	5.3	4.0	78.5	72.0	96.3	33.7	10.0	2.4%
6	RuAcNaC/MI386-35	408.8	261.8	6.7	4.3	67.4	26.8	94.5	29.1	11.4	2.8%
7	RuAcNaN/MI386-15	241.4	222.7	2.2	2.0	96.0	66.8	97.0	43.2	6.2	2.6%
12	RuAcNaN/MI386-27	372.4	279.7	5.2	3.9	80.1	30.0	93.4	36.2	13.4	3.6%
8	RuAcNaN/MI386-35	342.5	291.2	5.3	4.5	90.4	34.5	95.0	44.0	10.7	3.1%

[a] Estimated as the difference between the blank signal of 5% CO_2 and the CO_2 measured during the capture step
[b] $X_{CO2} = CH_4/(CO_2 \text{ captured} - CO_2 \text{ released})$
[c] Calculated as 80% of the CH_4 produced divided by the time required to reach that value
[d] $S_{CH4} = CH_4/(CO + CO_2 + CH_4)$

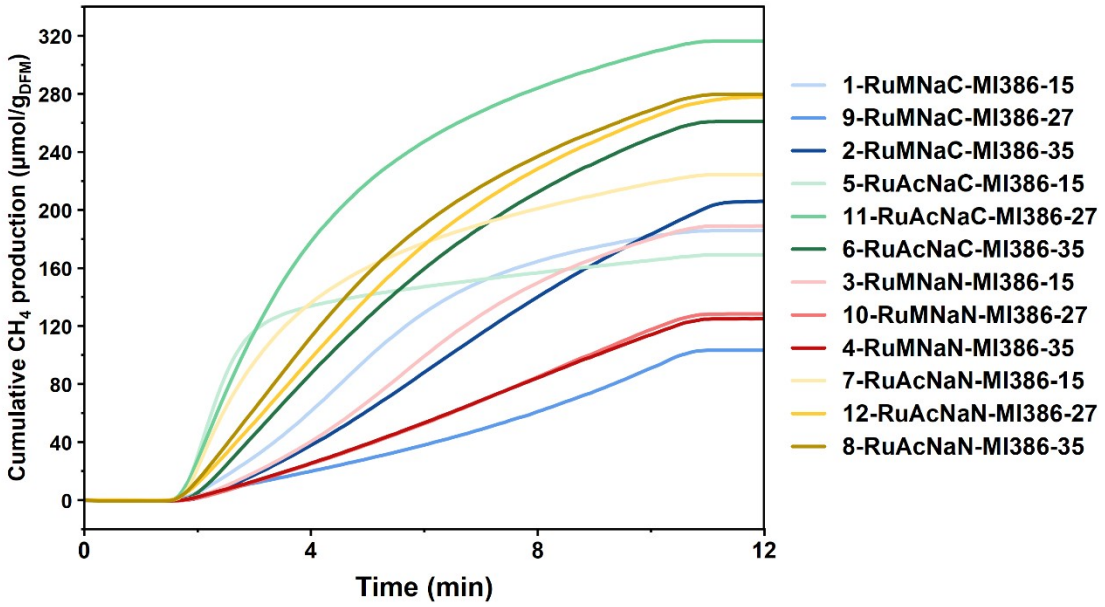

Figure S10. Cumulative CH_4 production during the 5th methanation step (350 °C, 10% H_2/N_2, 50 mL/min, 250 mg).

Table S3. Comparison of CO_2 capture capacity and CH_4 productivity of the best performing milled sample from this work with DFMs from the literature with comparable formulations based on Ru, Na and Al_2O_3.

Sample	Ru and Na_2O wt.% loading	Synthesis method	Reaction temperature [°C]	CO_2 captured [µmol/g_{DFM}]	CH_4 yield [µmol/g_{DFM}]	Ru specific CH_4 yield [mmol/g_{Ru}]	Reference
11-RuAcNaC/ MI386-27	1% Ru, 10% Na_2O	Dry ball milling	350	421	322	32.2	This work
Ru-16Na/Al_2O_3	4% Ru, 9.3% Na_2O	Wet impregnation	310	n.a.	310	7.8	[3]
Ru-Na/Al_2O_3	1% Ru, 4% Na_2O	Incipient wetness impregnation	350	47	47	4.7	[4]
5% Ru, 10% Na_2CO_3/Al_2O_3	5% Ru, 6.1% Na_2O	Incipient wetness impregnation	320	400	240	4.8	[5]
5%Ru – 6.1% "Na_2O"/Al_2O_3	5% Ru, 6.1% Na_2O	Incipient wetness impregnation	320	650	614	12.3	[6]
3Na-Ru/A	1% Ru, 4% Na_2O	Incipient wetness impregnation	300	297	207	20.7	[7]
3Na3Li-Ru/A	1% Ru, 4% Na_2O (+6.5% Li_2O)	Incipient wetness impregnation	360	427	322	32.2	[8]
RuNAl_PC	1%Ru, 12%Na_2O	Wet impregnation, Pechini method	350	700	450	45.0	[9]

The ANOVA tables (Analysis of Variance) show the components of the model used to analyse the results, the degrees of freedom (DF), sum of squares (Adj. SS), mean squares (Adj. MS), F-statistic, and p-values for each part of the model. The ANOVA tables help determine if there are significant differences between the averages of the groups being compared. The smaller the p-value, the more important or significant that part of the model is. In this study, a lower p-value indicates that a particular milling parameter has a stronger impact on the response being measured.

Table S4. ANOVA table for the average CO_2 capture capacity vs the milling intensity, the Na precursor and Ru precursor.

Source	DF	Adj SS	Adj MS	F-Value	p-value
Model	9	80244	8916	7.98	0.12
Linear	4	48560	12140	10.86	0.09
Milling intensity	2	41170	20585	18.42	0.05
Na precursor	1	2494	2494	2.23	0.27
Ru precursor	1	4896	4896	4.38	0.17
2-Way Interactions	5	31684	6337	5.67	0.16
Milling intensity*Na precursor	2	14232	7116	6.37	0.14
Milling intensity*Ru precursor	2	16293	8146	7.29	0.12
Na precursor*Ru precursor	1	1159	1159	1.04	0.42
Error	2	2235	1117		
Total	11	82479			

Table S5. ANOVA table for the average CH_4 production vs the milling intensity, the Na precursor and Ru precursor.

Source	DF	Adj SS	Adj MS	F-Value	p-value
Model	9	44799	4978	2.07	0.37
Linear	4	27232	6808	2.83	0.28
Milling intensity	2	3136	1568	0.65	0.61
Na precursor	1	73	73	0.03	0.88
Ru precursor	1	24022	24022	9.99	0.08
2-Way Interactions	5	17567	3513	1.46	0.45
Milling intensity*Na precursor	2	2153	1077	0.45	0.69
Milling intensity*Ru precursor	2	14441	7221	3	0.25
Na precursor*Ru precursor	1	973	973	0.4	0.59
Error	2	4809	2405		
Total	11	49608			

Table S6. ANOVA table for the average CO_2 conversion vs the milling intensity, the Na precursor and Ru precursor.

Source	DF	Adj SS	Adj MS	F-Value	p-value
Model	9	3424	380	3.63	0.23
Linear	4	3109	777	7.42	0.12
Milling intensity	2	1758	879	8.4	0.11
Na precursor	1	3	3	0.03	0.88
Ru precursor	1	1348	1348	12.87	0.07
2-Way Interactions	5	315	63	0.6	0.72
Milling intensity*Na precursor	2	288	144	1.38	0.42
Milling intensity*Ru precursor	2	26	13	0.12	0.89
Na precursor*Ru precursor	1	1	1	0.01	0.92
Error	2	209	105		
Total	11	3634			

Table S7. ANOVA table for the CH_4 selectivity vs the milling intensity, the Na precursor and Ru precursor.

Source	DF	Adj SS	Adj MS	F-Value	p-value
Model	9	710752	78972	1.61	0.44
Linear	4	546455	136614	2.78	0.28
Milling intensity	2	149848	74924	1.53	0.40
Na precursor	1	5077	5077	0.1	0.78
Ru precursor	1	391530	391530	7.97	0.11
2-Way Interactions	5	164298	32860	0.67	0.69
Milling intensity*Na precursor	2	54056	27028	0.55	0.65
Milling intensity*Ru precursor	2	95817	47909	0.98	0.51
Na precursor*Ru precursor	1	14425	14425	0.29	0.64
Error	2	98192	49096		
Total	11	808945			

Table S8. ANOVA table for the CH_4 release rate vs the milling intensity, the Na precursor and Ru precursor.

Source	DF	Adj SS	Adj MS	F-Value	p-value
Model	9	8320.1	924.5	5.17	0.17
Linear	4	6982.1	1745.5	9.76	0.10
Milling intensity	2	1203.2	601.6	3.36	0.23
Na precursor	1	288.5	288.5	1.61	0.33
Ru precursor	1	5490.4	5490.4	30.69	0.03
2-Way Interactions	5	1338	267.6	1.5	0.45
Milling intensity*Na precursor	2	263.9	131.9	0.74	0.58
Milling intensity*Ru precursor	2	893.2	446.6	2.5	0.29
Na precursor*Ru precursor	1	181	181	1.01	0.42
Error	2	357.8	178.9		
Total	11	8677.9			

Table S9. ANOVA table for the CO release during the CO_2 capture vs the milling intensity, the Na precursor and Ru precursor.

Source	DF	Adj SS	Adj MS	F-Value	p-value
Model	9	709611	78846	1.01	0.59
Linear	4	309899	77475	0.99	0.56
Milling intensity	2	28199	14099	0.18	0.85
Na precursor	1	2241	2241	0.03	0.88
Ru precursor	1	279460	279460	3.57	0.20
2-Way Interactions	5	399712	79942	1.02	0.56
Milling intensity*Na precursor	2	67170	33585	0.43	0.70
Milling intensity*Ru precursor	2	58796	29398	0.38	0.73
Na precursor*Ru precursor	1	273745	273745	3.5	0.20
Error	2	156590	78295		
Total	11	866201			

Table S10. ANOVA table for the CO_2 release during the methanation vs the milling intensity, the Na precursor and Ru precursor.

Source	DF	Adj SS	Adj MS	F-Value	p-value
Model	9	311753	34639	1.18	0.54
Linear	4	240118	60029	2.05	0.35
Milling intensity	2	76590	38295	1.31	0.43
Na precursor	1	7210	7210	0.25	0.67
Ru precursor	1	156318	156318	5.34	0.15
2-Way Interactions	5	71636	14327	0.49	0.78
Milling intensity*Na precursor	2	38628	19314	0.66	0.60
Milling intensity*Ru precursor	2	6300	3150	0.11	0.90
Na precursor*Ru precursor	1	26709	26709	0.91	0.44
Error	2	58526	29263		
Total	11	370279			

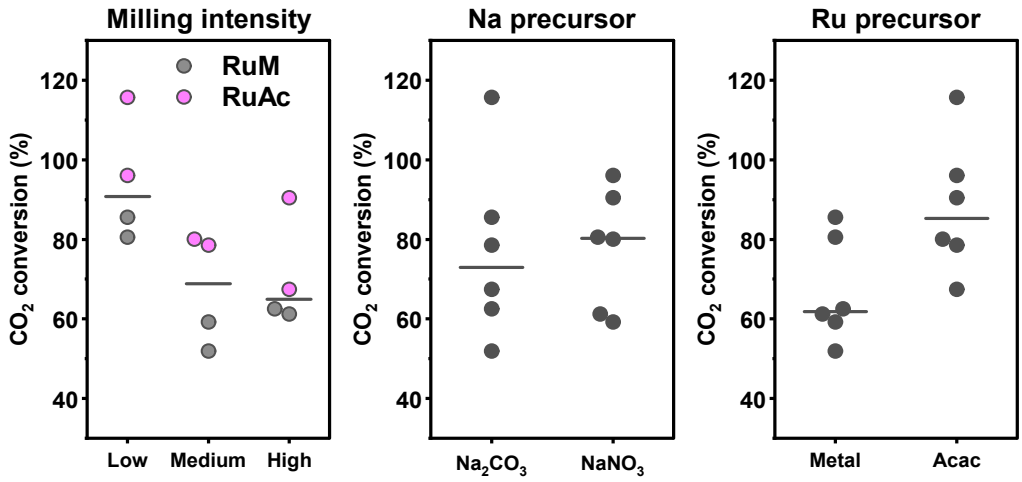

Figure S11. Main effect plots of the CO_2 conversion at the different milling parameters.

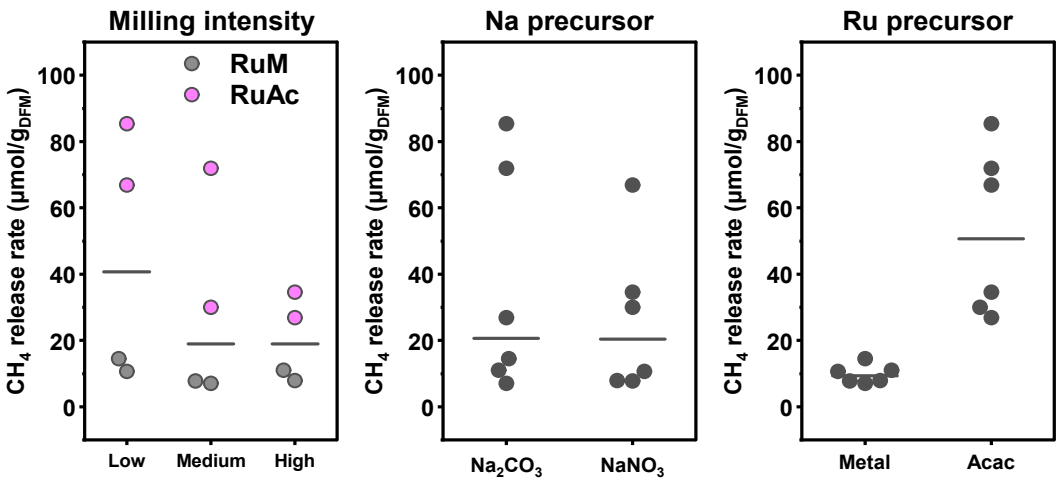

Figure S12. Main effect plots of the CH_4 release rate at the different milling parameters.

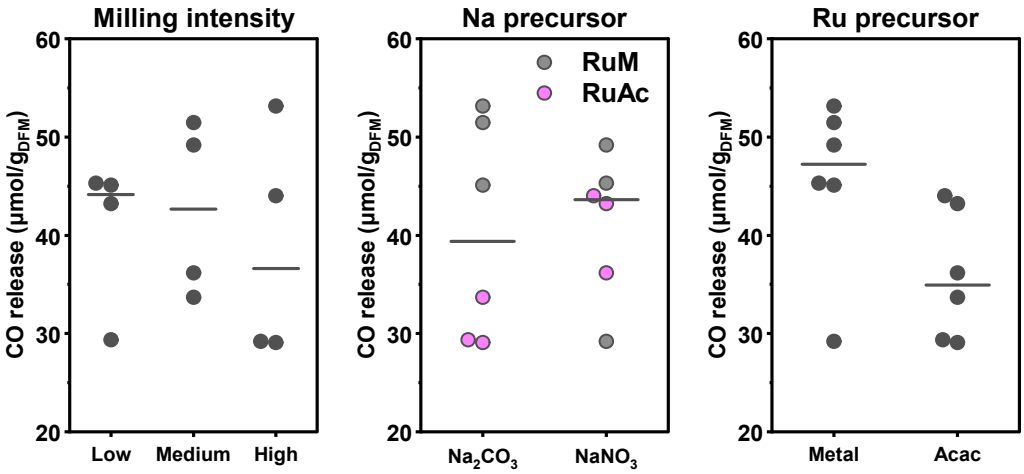

Figure S13. Main effect plots of the CO released during the CO_2 capture step at the different milling parameters.

Spent DFMs characterisation

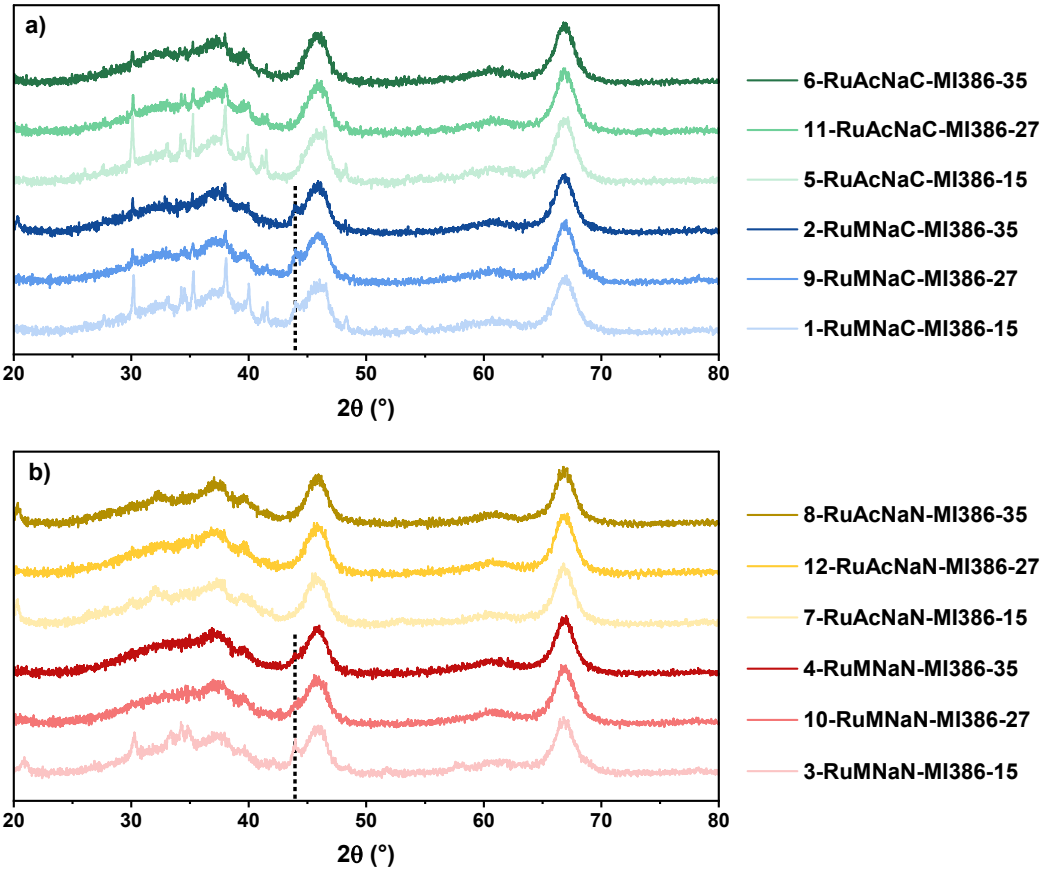

Figure S14. XRD diffractograms of the spent DFMs of **a)** Na_2CO_3-based DFMs and **b)** $NaNO_3$-based DFMs. The dashed line represents the position of the metallic Ru(101) peak at 44.0° 2θ.

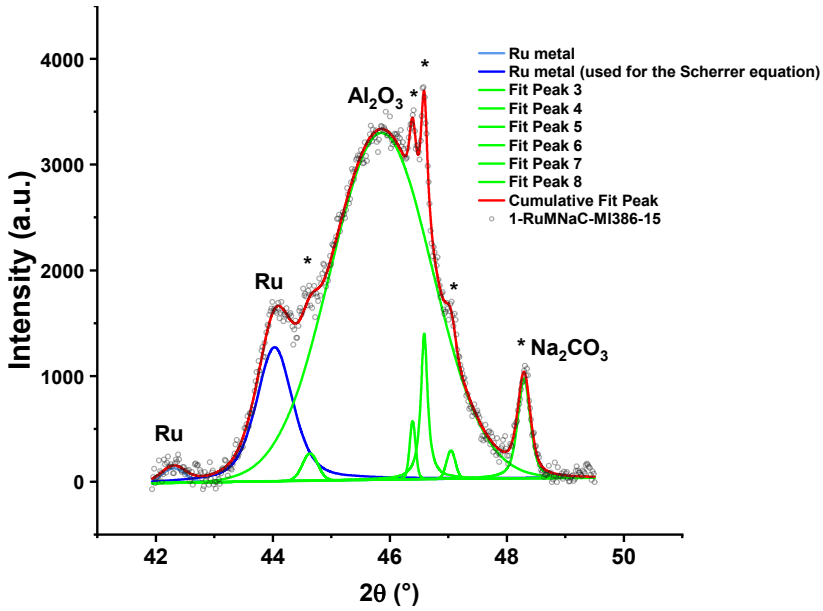

Sample	Ru crystallite size (nm)
1-RuMNaC/MI386-15	11.7
9-RuMNaC/MI386-27	12.8
2-RuMNaC/MI386-35	13.2
3-RuMNaN/MI386-15	15.3
10-RuMNaN/MI386-27	11.3
4-RuMNaN/MI386-35	16.6

Figure S15. Example of the peak structure deconvolution of the spent 1-RuMNaC/MI386-15 for the Ru crystallite size estimation and values estimated with the Scherrer equation.

References

1 T. S. Nguyen, L. Lefferts, K. B. Saisankargupta and K. Seshan, *ChemCatChem*, 2015, **7**, 1833–1840.

2 C. J. Keturakis, F. Ni, M. Spicer, M. G. Beaver, H. S. Caram and I. E. Wachs, *ChemSusChem*, 2014, **7**, 3459–3466.

3 A. Bermejo-López, B. Pereda-Ayo, J. A. Onrubia-Calvo, J. A. González-Marcos and J. R. González-Velasco, *J. CO2 Util.*, 2022, **58**, 1–11.

4 A. Porta, R. Matarrese, C. G. Visconti, L. Castoldi and L. Lietti, *Ind. Eng. Chem. Res.*, 2021, **60**, 6706–6718.

5 S. Wang, E. T. Schrunk, H. Mahajan and R. J. Farrauto, *Catalysts*, 2017, **7**, 1–13.

6 M. A. Arellano-Treviño, Z. He, M. C. Libby and R. J. Farrauto, *J. CO2 Util.*, 2019, **31**, 143–151.

7 S. Cimino, E. M. Cepollaro and L. Lisi, *Appl. Catal. B Environ.*, 2022, **317**, 121705.

8 S. Cimino, E. M. Cepollaro, F. Frusteri and L. Lisi, *Sep. Purif. Technol.*, 2025, **354**, 129101.

9 A. I. Tsiotsias, N. D. Charisiou, A. G. S. Hussien, A. A. Dabbawala, V. Sebastian, K. Polychronopoulou and M. A. Goula, *J. Environ. Chem. Eng.*, 2024, **12**, 112712.